frontiers | Frontiers in Immunology

TYPE Original Research
PUBLISHED 26 June 2023
DOI 10.3389/fimmu.2023.1212770

OPEN ACCESS

EDITED BY
Fuminori Tokunaga,
Osaka Metropolitan University, Japan

REVIEWED BY
Monisankar Ghosh,
Stony Brook University, United States
Istvan Boldogh,
University of Texas Medical Branch at Galveston, United States

*CORRESPONDENCE
Allan R. Brasier
abrasier@wisc.edu

†PRESENT ADDRESS
David S. Roberts,
Department of Chemistry and Sarafan ChEM-H, Stanford University, Stanford, CA, United States

RECEIVED 26 April 2023
ACCEPTED 05 June 2023
PUBLISHED 26 June 2023

CITATION
Mann MW, Fu Y, Gearhart RL, Xu X, Roberts DS, Li Y, Zhou J, Ge Y and Brasier AR (2023) Bromodomain-containing Protein 4 regulates innate inflammation via modulation of alternative splicing.
Front. Immunol. 14:1212770.
doi: 10.3389/fimmu.2023.1212770

Bromodomain-containing Protein 4 regulates innate inflammation via modulation of alternative splicing

Morgan W. Mann[1], Yao Fu[1], Robert L. Gearhart[2], Xiaofang Xu[1], David S. Roberts[2†], Yi Li[3], Jia Zhou[3], Ying Ge[2,4,5] and Allan R. Brasier[1,6*]

[1]Department of Medicine, University of Wisconsin – Madison, Madison, WI, United States, [2]Department of Chemistry, University of Wisconsin – Madison, Madison, WI, United States, [3]Department of Pharmacology and Toxicology, University of Texas Medical Branch, Galveston, TX, United States, [4]Department of Cell and Regenerative Biology, University of Wisconsin-Madison, Madison, WI, United States, [5]Human Proteomics Program, University of Wisconsin-Madison, Madison, WI, United States, [6]Institute for Clinical and Translational Research, University of Wisconsin-Madison, Madison, WI, United States

Introduction: Bromodomain-containing Protein 4 (BRD4) is a transcriptional regulator which coordinates gene expression programs controlling cancer biology, inflammation, and fibrosis. In the context of airway viral infection, BRD4-specific inhibitors (BRD4i) block the release of pro-inflammatory cytokines and prevent downstream epithelial plasticity. Although the chromatin modifying functions of BRD4 in inducible gene expression have been extensively investigated, its roles in post-transcriptional regulation are not well understood. Given BRD4's interaction with the transcriptional elongation complex and spliceosome, we hypothesize that BRD4 is a functional regulator of mRNA processing.

Methods: To address this question, we combine data-independent analysis - parallel accumulation-serial fragmentation (diaPASEF) with RNA-sequencing to achieve deep and integrated coverage of the proteomic and transcriptomic landscapes of human small airway epithelial cells exposed to viral challenge and treated with BRD4i.

Results: We discover that BRD4 regulates alternative splicing of key genes, including Interferon-related Developmental Regulator 1 (IFRD1) and X-Box Binding Protein 1 (XBP1), related to the innate immune response and the unfolded protein response (UPR). We identify requirement of BRD4 for expression of serine-arginine splicing factors, splicosome components and the Inositol-Requiring Enzyme 1 IREα affecting immediate early innate response and the UPR.

Discussion: These findings extend the transcriptional elongation-facilitating actions of BRD4 in control of post-transcriptional RNA processing via modulating splicing factor expression in virus-induced innate signaling.

KEYWORDS

BRD4, innate inflammatory response, alternative splicing, unfolded protein response, IFRD1, RSV (respiratory syncytial virus)

Introduction

Bromodomain-containing protein 4 (BRD4) is a key regulator of development, tumorigenesis, inflammation, and fibrosis in mammalian organisms (1–5). In the context of airway inflammation, aeroallergens and airway pathogens trigger NF-κB/BRD4-mediated innate inflammation *via* activation of upstream pattern recognition receptors (6). These include the toll-like receptors (TLRs) and the RIG-Helicase (RIGI), which induce the proteolytic degradation of the NF-κB inhibitory subunit (NFκBIA), resulting in cytoplasmic release and nuclear translocation of NF-κB subunit p65 (RelA), where it interacts with BRD4 and the latent positive transcription elongation factor (pTEFb) (7). Upon BRD4 binding, pTEFb dissociates from inhibitory 7SK RNA/HEXIM, and the resulting complex phosphorylates promoter-proximal paused RNA polymerases and negative elongation factors. In this way, PTEFb produces rapid transcriptional elongation of fully spliced, immediate-early NF-κB-dependent genes, resulting in rapid and efficient activation of pro-inflammatory cytokines, chemokines, and anti-viral interferons. This process provides a key initial barrier to viral infection, and recruits a robust cellular immune response for prolonged protection by stimulating adaptive immunity. Additionally, prolonged BRD4 activation results in epithelial plasticity, basement membrane remodeling, and fibrosis (8).

BRD4 derives its name and primary function from its tandem, acetyl-lysine binding bromodomains (BDs), which facilitate interactions with acetylated histones and other acetylated proteins (6, 9, 10). This characteristic enables BRD4 to bind tightly to transcriptionally active DNA, serving as an epigenetic "bookmark" (11). Protein interaction studies have observed that BRD4 binds not only to acetylated NF-κB p65/RelA, but forms a dynamic multi-component complex with the AP-1 transcription factors, members of the Mediator complex, SWI-SNF chromatin-remodeling complex, and RNA-splicing factors (12, 13). Understanding the BRD4 protein-protein interaction network provides novel insights into the pleiotropic functions of the BRD4 complex.

The development of potent and selective small-molecule inhibitors of the BRD4 BDs has enabled systematic interrogation of dynamic BRD4-acetylated protein interactions (12). Interestingly, BRD4 interactions with members of the spliceosome complex can be disrupted by inhibitors of the acetyl-lysine binding pocket. The spliceosome is a multi-megadalton complex of 5 small nuclear RNAs (snRNAs) and approximately 100 proteins that function together to process messenger RNA precursors (pre-mRNA) and process them into mature mRNA (14). This involves catalytic removal of non-protein coding intronic regions of the pre-mRNA, and re-ligation into a contiguous, translatable mRNA. Key protein subunits of the spliceosome include the small nuclear ribonucleoproteins (snRNPs) U1 and U2, which form a pre-spliceosome complex at the sites of intronic regions, and the U4, U5, and U6 snRNPs which complete the spliceosome and initiate splicing through a U2/U6-dependent mechanism (15, 16). Numerous additional snRNPs and splicing factors contribute structural and functional roles to the complex, coupling mRNA splicing to processes such as transcription and mRNA export (17, 18). Alternative splicing of exon regions (also known as exon-skipping) is also possible, and gives rise to significant diversity in the transcriptome (19). Importantly, the role of BRD4 in alternative splicing is not fully understood.

Respiratory Syncytial Virus (RSV) is an enveloped, single-stranded, negative-sense RNA virus that is the largest cause of pediatric hospitalizations worldwide (20, 21). RSV thus represents a significant burden on healthcare systems, especially as cases surged in the wake of the SARS-CoV-2 pandemic (22). RSV infects the epithelial cells of the respiratory tract, and induces rapid activation of the NFκB-BRD4-PTEFb pathway (2, 6, 12, 23–27). Previous RNA sequencing studies have discovered that replication of RSV and other paromyxoviruses induce substantial alternative splicing events, including intron retention, exon skipping, and alternative polyadenylation site utilization (28, 29). However, the mechanisms by which RSV induces alternative splicing are not known.

In this study, we investigate BRD4-mediated alternative splicing in the context of RSV-induced innate inflammation, using a multi-omics approach combining in-depth short-read RNA-sequencing with high-throughput trapped ion mobility (TIMS) mass spectrometry. This combined approach enables a deep profiling of both the transcript- and protein-level abundance changes that result from alternative splicing events. Our results demonstrate that BRD4 regulates RSV-induced intron retention, consequently modulating the abundance of associated co-regulators of innate inflammation. Furthermore, we demonstrate that these changes result in decreased activation of NFκB-mediated gene expression, independent of BRD4 inhibition.

Materials and methods

Reagents

The BRD4-selective BD competitive inhibitor, ZL0454, was synthesized as previously described (30, 31), and determined to be >99% pure. The 4-hexylphenylazosulfonate (Azo) used in these experiments was synthesized in-house as described previously (32, 33). The sources of all other reagents and kits are provided in Table S1.

Biological resources

Virus preparation

The human RSV long strain was grown in Hep-2 cells and prepared by sucrose gradient centrifugation as previously described (6, 34–36). The viral titer of purified RSV pools was varied from 8 to 9 log PFU/ml, determined by a methylcellulose plaque assay (36, 37). Viral pools were aliquoted, quick-frozen on dry ice-ethanol, and stored at −70°C until used.

Cell culture

Primary human small airway epithelial cells (hSAECs) were immortalized using human Telomerase/CDK4 as previously described (38, 39), and grown in SAGM small airway growth medium (Lonza, Walkersville, MD, USA). A549 alveolar epithelial

cells were purchased from the American Type Culture Collection (ATCC, Manassas, Virginia, USA), and grown in F12K medium supplemented with 10% fetal bovine serum. All cells were incubated at 37°C, 5% CO_2 until confluence

ZL0454 was dissolved in dimethylsulfoxide (DMSO) and added to the relevant cell culture media at a final concentration of 10 μM. The ZL0454 inhibitor or vehicle (DMSO) was added 18 hours before infection/stimulation, and to the media during infection/stimulation. hSAECs were infected with viral particles at a multiplicity of infection (MOI) of 1, or left uninfected (Mock). hSAECs were harvested at 24 hours post-infection.

Polyinosinic-polycytidilyic acid (polyIC) was reconstituted in phosphate-buffered saline (PBS) at a concentration of 10 mg/ml. Reconstituted polyIC was added to cell culture medium at a final concentration of 50 μg/ml, and consequently added to hSAECs for stimulation. PBS was used as a vehicle control. hSAECs were stimulated with polyIC for 15, 30, or 60 minutes before harvest.

siRNA knockdown

Non-targeting (Cat. # T-2001-01) and IFRD1-specific (Cat. # L-019615-00-0005) ON-TARGETplus SMARTPool siRNA was purchased from Horizon Discovery Biosciences (Cambridge, UK). Target sequences are described in Table S2. siRNA was transfected into hSAECs as per the manufacturer's instructions, and cells were harvested for protein and RNA 72 hours later.

Method details

Proteomics sample preparation

Human small airway epithelial cells (hSAECs) were lysed in a buffer containing 0.2% Azo, 25mM Ammonium Bicarbonate, 10 mM L-Methionine, 1 mM Dithiothreitol (DTT), 1x HALT Protease and Phosphatase Inhibitor (Thermofisher, Waltham, MA, USA, Cat. # 78440), before transfer to microcentrifuge tubes and boiling at 95°C for 5 minutes. Samples were diluted to 0.1% Azo, and standardized to 0.5 mg/ml by Bradford Assay (Bio-Rad, Hercules, CA, USA, Cat. # 5000006), prior to chemical reduction using 30 mM DTT for 60 minutes at 37°C. Freshly prepared iodoacetamide solution (200 mM) was added to a final concentration of 20 mM, and the samples were incubated in the dark for 30 min. Protein was digested with Trypsin Gold (Promega, Madison, WI, USA) at a 1:50 enzyme:protein ratio overnight at 37°C with agitation at 1000 rpm.

Digestion was quenched by addition of formic acid to a final concentration of 1%, and irradiated at 305 nM for 5 minutes to photocleave the Azo surfactant. Samples were centrifuged at 15,000xg, and supernatents were desalted using Pierce C18 tips (ThermoScientific, Waltham, MA, USA). Peptide pellets were resuspended in 0.2% Formic Acid immediately prior to LC-MS analysis.

Online data independent analysis - parallel accumulation serial fragmentation label-free quantitative proteomics

Desalted peptides (200 ng) were loaded and separated on an IonOptiks Aurora UHPLC column with CSI fitting (Melbourne, Australia) at a flow rate of 0.4 μL/min and a linear gradient increasing from 0% to 17% mobile phase B (0.1% formic acid in acetonitrile) (mobile phase A: 0.1% formic acid in water) over 60 min; 17% to 25% from 60 to 90 min; 25% to 37% B from 90 to 100 min; 37% to 85% B from 100 min to 110 min; and a 10 min hold at 85% B before washing and returning to low organic conditions. The column directly integrated a nanoESI source for delivery of the samples to the mass spectrometer. MS spectra were captured with a timsTOF Pro quadrupole-time of flight (Q-TOF) mass spectrometer (Bruker Daltonics, Billerica, MA, USA) operating in diaPASEF mode, using 32 windows ranging from m/z 400 to 1200 and $1/K_0$ 0.6 to 1.42. Precise windows settings are available in the Table S3.

RelA immunoprecipitation

A549 alveolar epithelial cells were lysed in Low Ionic Strength Immunoprecipitation Buffer (50 mM NaCl, 10 mM HEPES, 1% Triton-X100, 10% Glycerol) with 1 mM DTT and 1% Protease Inhibitor Cocktail (MilliporeSigma, Burlington, MA, USA, Cat. # P8340), and extracts were sonicated 3x for 10 seconds each time (BRANSON Sonifier 150, setting 4) prior to centrifugation at 10000xg, 4°C for 10 minutes. Supernatants were collected, and total protein abundance was normalized to 2 μg using the Detergent-compatible Protein Assay (Biorad, Hercules, CA, USA, Cat. # 5000111). 2 μg α-RelA antibody (Cell Signaling, Danvers, MA, USA, Cat. # 8242) was added to each extract, and the samples were incubated overnight at 4°C with rotation.

The next day, 30 μl Protein G-conjugated magnetic beads (Dynabeads, Invitrogen, Waltham, MA, USA, Cat. # 10003D) were added to each sample and allowed to bind for 4 hours at 4°C. After binding, supernatents were removed, and the beads were washed 3x in Low Ionic Strength Immunoprecipitation Buffer, prior to elution by boiling in 2x Laemli loading buffer (BioRad, Hercules, Ca, USA, Cat. # 1610737EDU) at 95°C for 5 minutes. Eluate was examined by western blot, as detailed in the next section.

Western blotting

For total protein quantitation, cells were lysed and protein extracted using radio-immunoprecipitation buffer (50 mM Tris-HCL (pH 7.6), 150 mM NaCl 1% NP-40, 0.5% Sodium Deoxycholate, 0.1% SDS) with 1 mM Dithithreitol and 1x Protease Inhibitor Cocktail(MilliporeSigma, Burlington, MA, USA, Cat. # P8340) added. Protein was normalized using the Detergent-compatible Protein Assay (Biorad, Hercules, CA, USA, Cat. # 5000111), and loaded onto a 4–20% Criterion TGX Precast Protein Gel (Biorad, Hercules, CA, USA) for separation. Immunoprecipitation samples were prepared as detailed in the previous section.

Proteins were transferred to a nitrocellulose membrane using a Trans-Blot Turbo Transfer System (Biorad, Hercules, CA, USA) with a constant voltage of 25 V over 30 min. The membrane was blocked for 1 h using 5% milk powder in Tris-buffered Saline with 0.1% Tween-20 (TBST) and incubated overnight at 4°C with primary antibody (see Table S1) diluted in 5% milk powder in

TBST. Membranes were washed thoroughly and incubated with a horseradish peroxidase (HRP)-conjugated secondary antibody diluted 1:200,000 in 5% milk powder in TBST for 1 hour at room temperature. The VeriBlot IP Detection Reagent (1:200 dilution, Abcam, Cambridge, UK, Cat. # ab131366) was used as a secondary antibody for immunoprecipitated samples. Imaging was performed *via* chemiluminescent detection using Supersignal West Femto Maximum Sensitivity Substrate (ThermoFisher, Waltham, MA, USA, Cat. # 34095) and an Azure c500 gel imaging system (Azure Biosystems, Dublin, CA, USA). When necessary, bands were quantified by densitometry, using FIJI version 1.53c (40). Membranes were stripped between incubation with different antibodies using Restore Western Blot Stripping Buffer (ThermoFisher, Waltham, MA, USA, Cat. # 21059).

RNA isolation and reverse-transcriptase PCR

Cellular RNA from cultured cells was isolated using an RNeasy kit with on-column DNase digestion (Qiagen, Germantown, MD, USA, Cat. # 74004). RNA was reverse transcribed into cDNA using the First Strand cDNA Synthesis kit (Thermo Fisher Scientific). Quantitative PCR (qPCR) reactions were conducted in duplicate using SYBR Green Master mix (Bio-Rad) and 500 ng of cDNA in 20 ul reactions. Gene-specific primers were used at a concentration of 500 nM and are listed below. The qPCR reaction was carried out on a AriaMx Real-Time PCR System (Agilent, Santa Clara, CA, USA) with 40 cycles of 15 seconds at 95°C and 30 seconds at 60°C. Cyclophilin A (PP1A) was used as a housekeeping gene for overall gene expression. XBP1-Total was used to normalize the abundance of spliced XBP1 (XBP1-Short).

IFRD1 splicing variants were amplified using Q5 High Fidelity Polymerase (New England Biolabs, Ipswich, MA, USA, Cat. # M0491S) on an AriaMX Real-Time PCR System (Agilent, Santa Clara, CA, USA) with 35 cycles of 10 seconds at 98°C, 30 seconds at 67°C, and 30 seconds at 72°C. Due to the significant heterogeneity of IFRD1 transcript variants, primers for total IFRD1 (IFRD1-Total) were chosen amplify a common region, bridging exons 7 and 8, found in all protein-coding transcripts. The expected amplification products (IFRD1-204: 707, IFRD1-Total: 201 bp) were imaged *via* UV detection on an Azure c500 gel imaging system (Azure Biosystems, Dublin, CA, USA), and quantified by Gel Densitometry.

Two-step crosslinking chromatin immunoprecipitation - PCR

Cells were cross-linked *in-vivo* using disucinimidylglutarate (DSG) and methanol-free formaldehyde as previously described (41). After lysis (1% SDS, 50 mM Tris-HCl, pH 8.0), extracts were sonicated 3x for 10 seconds each time (BRANSONSonifier 150, setting 4), and centrifuged for 5 min at 10,000 g, 4°C. Supernatents were diluted 10-fold in Low Ionic Strength Immunoprecipitation Buffer (50 mM NaCl, 10 mM HEPES, 1% Triton-X100, 10% Glycerol) with 1 mM DTT and 1% Protease Inhibitor Cocktail (MilliporeSigma, Burlington, MA, USA, Cat. # P8340). Constant volumes of sample were incubated overnight with 2 μg α-BRD4 antibody (Cell Signaling, Danvers, MA, USA, Cat. # 13440) or a nonspecific isotype control (LSBio, Seattle, WA,USA, Cat. # LS-C149375).

The next day, 20 μl Protein G-conjugated magnetic beads (Dynabeads, Invitrogen, Waltham, MA, USA) were added to each sample and incubated for 1 hour at 4°C. 50 μl aliquots were taken from each sample to serve as Input controls. All samples were washed twice in Low Ionic Strength IP buffer, once in High Ionic Strength Wash Buffer (500 mM NaCl, 0.1% SDS, 1% Triton-X100, 2 mM EDTA, 20 mM Tris-HCl, pH 8.0), and twice in Tris-EDTA Buffer (10 mM Tris-HCl, 1 mM EDTA, pH 8.0) prior to elution in 300 μl 0.1 M Sodium Bicarbonate, 1% SDS at 65°C. Samples were decrosslinked *via* the addition of 20 μg Proteinase K, and incubated overnight at 65°C.

Decrosslinked DNA was purified by Phenol-Chloroform Extraction and Ethanol Precipitation. In brief, 100 μl of 5:1 Phenol : Chloroform was added to each sample prior to vortexing, and centrifugation at 14000xg, 24°C for 10 minutes. The supernatent was transferred to a new tube containing 100 μl of chloroform, and vortexed and centrifuged again as above. Finally, the supernatents (~200 μl) were transferred to a new tube containing 100 μl 7.5 M Ammonium Acetate and 60 μg of glycogen.1 ml of 100% ethanol was added to each tube, and the samples were vortexed prior to overnight precipitation at -80°C. Purified DNA was reconstituted with DNase-free water, and quantified by qPCR. Input control samples were used for normalization.

Quantitation and statistical analysis

Short-read RNA sequencing and splicing analysis

RNA-Sequencing (RNA-Seq) data was obtained from Xu et. al (28). The data was analyzed using R version 4.1.0 and the "IsoformSwitchAnalyzeR" R Package (42), utilizing Gencode version 33 transcripts (43), and integrating the "CPAT" (44), "PFAM" (45), "SignalP" (46), and "IUPRED2A" (47) tools to characterize transcripts based on coding status and switch consequence. Isoform switches were identified using an isoform switch q-value threshold of 0.05 and an isoform fraction difference of 0.1. Significant results were submitted to PANTHER gene list statistical over-representation test, using "PANTHER Biological Process Complete" as the annotation terms, and the Homo Sapiens genome as the reference list (48, 49). Gene ontology and annotation terms were filtered to a 1% false discovery rate (FDR). Comparison of protein and transcript-level data omitted the mock-infected/ZL0454-treated condition, as corresponding data was not collected in Xu et. al (28). Figures were generated using the "ggplot2" (50) and "ggpubr" (51) R packages for R version 4.1.0 (52). Boxplots represent the median and interquartile range of n=4 biological replicates.

Protein-level differential abundance analysis

Raw LC-MS data was quantified using DIA - Neural Network (DIANN) version 1.8 (53), using the following parameters: 1% FDR, Library-free search enabled, Minimum fragment m/z: 200, Maximum fragment m/z: 1800, Minimum precursor m/z: 400, Maximum precursor m/z: 1200, Minimum precursor charge: 2, Maximum precursor charge: 4, Minimum peptide length: 7, maximum peptide length: 30, Enzyme: Trypsin, N-terminal methionine cleavage enabled, cysteine carbamidomethylation enabled, Maximum missedcleavages: 1, MS1/MS2 mass accuracy: 10 ppm, Quantification strategy: Robust LC (High Precision), Neural network classifier: Double-pass mode. All other settings were left at default values. Data was searched against a fasta-formatted text file containing 20,404 reviewed human protein sequences (Taxon ID: 9606) and 6 sequences from the RSV Long-strain (Taxon ID: 11260) (54).

Protein-level quantification data was filtered using the "DAPAR" package (55) for R version 4.1.0 to include all proteins quantified in 2 of 3 runs in at least one sample group. Values were then median normalized and missing values were imputed *via* ssla for partially observed values within a condition, or set to the 2.5% quantile of observed intensities for observations that were missing entirely within a condition. The "DEP" R package (56) was used to perform a Limma test between all specified contrasts, and the "IHW" R package (57) was used to adjust all p-values, using the number of quantified peptides per protein as a covariate. A P_{Adj} threshold of 0.05 and a Log_2 Fold Change threshold of 0.6 were set to identify significant changes to protein abundance. Tandem MS spectra were visualized and plotted using Skyline (58) and the "ggplot2" (50) package for R version 4.1.0 (52). Boxplots were generated using the "ggpubr" (51) package for R version 4.1.0 (52).

Gel densitometry

Gel bands were quantified using FIJI version 1.53c (40), and statistical analysis was conducted by One- or Two-Factor ANOVA, with *post-hoc* Tukey's HSD. Boxplots were generated using the "ggpubr" (51) package for R version 4.1.0 (52). Boxplots represent median and interquartile range of n=3 biological replicates. Barplots represent mean ± standard error (SE) of n=3 biological replicates.

qPCR quantification and analysis

Data was analyzed using the ΔΔCt method. Statistical analysis was conducted by Two-Factor ANOVA and *post-hoc* Tukey's HSD. Boxplots were generated using the "ggpubr" (51) package for R version 4.1.0 (52), and represent median and interquartile range of n=3 biological replicates. Scatter plots represent mean ± standard error (SE) of n=3 biological replicates.

Web sites

The PANTHER Classification System (48, 49) was used in the analysis of our datasets.

Results and discussion

BRD4 inhibition alters transcriptome-wide intron-retention and ORF length in airway epithelial cells

To investigate the effects of BRD4 inhibition and viral infection on alternative splicing in the airway epithelium, we analyzed data from *Xu et. al (28).* to discover alternative splicing events. This data was collected in telomerase-immortalized human airway epithelial cells (hSAECs) that had been treated with the specific BRD4 inhibitor ZL0454 18 hours prior to and during 24 hours of infection with Respiratory Syncytial Virus (n=4 per group, Multiplicity of Infection of 1). hSAECs are a well-established airway epithelial model derived from bronchioles that represent a primary arm of the innate response to RNA virus infection (34, 60). These cells maintain stable epithelial morphology inmonoculture, and reproduce both genomic and proteomic signatures of primary cells without early senescence (25). ZL0454 is a potent competitive BD inhibitor highly selective for BRD4 over other members of the bromodomain family (30, 61).

This alternative spliceform analysis revealed 2001 genes and over 3635 unique transcripts with significant ($Q_{Val} < 0.05$, $|dIF| > 0.1$) isoform switching events in at least one comparison between experimental groups. 1008 genes had induced isoform switching due to RSV infection, and 822 genes were associated with isoform switching due to BRD4 inhibition in RSV-infected cells (Figure 1). BRD4 Inhibitor (BRD4i)-associated splicing events were subjected to PANTHER gene ontology analysis (48, 49), indicating significant changes to kinetochore assembly and nucleic-acid/base-pair metabolism. 314 genes overlapped between conditions, suggesting switch events regulated by both RSV and BRD4, however, no PANTHER ontology terms were significantly enriched among these genes. We conclude that BRD4 does not alter alternative splicing in a pathway-concerted manner. Splicing events were further analyzed by association with transcript-level features. RSV-induced splicing events were associated with predominantly shorter Open Reading Frames (ORFs) and noncoding transcripts. In contrast, BRD4 inhibition reversed this pattern, and led to predominantly longer ORFs and retention of intronic regions. A full list of detected transcripts and splicing events is available in Table S4.

BRD4 regulates alternative splicing of key innate inflammation co-regulators

Manual evaluation of this dataset revealed that BRD4i was associated with sequence retention in several genes of note: X-box Binding Protein 1 (*XBP1*) and Interferon-related Developmental Regulator 1 (*IFRD1*) (Figure 2). The *XBP1* gene codes for a key transcription factor in the unfolded protein response (62), but must first be spliced to an active form, *XBP1s*, *via* the excision of a 26 nucleotide sequence (63). This results in a frame shift that allows the mRNA to be translated into the functional transcriptional regulator. XBP1 has been shown to activate expression of the Interleukin-6

10.3389/fimmu.2023.1212770

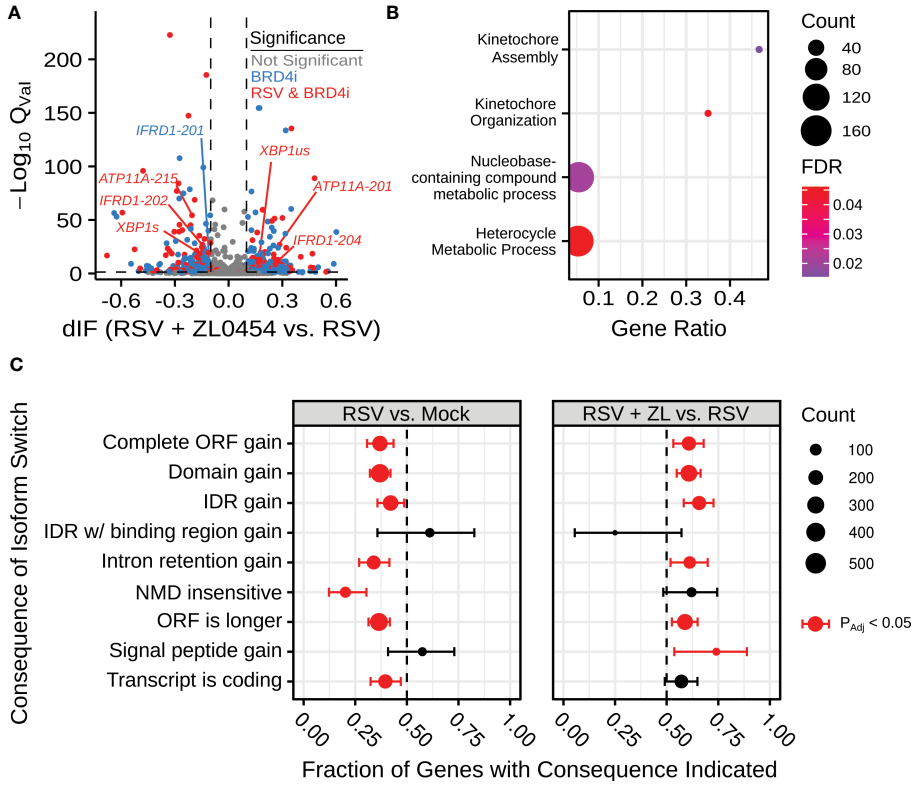

FIGURE 1
BRD4 inhibition alters alternative splicing in the context of airway viral infection. **(A)** Volcano plot indicating differential isoform fraction (dIF) and isoform switch q-value of isoform switching events with predicted gene-level consequences. Non-significant changes (Q_{Val} >.05 or |dIF| < 0.1 are plotted in grey. Significant changed transcripts also found to be significantly changed due to RSV-infection are plotted in red. Significant switch events only detected due to BRD4 inhibition are plotted in blue. **(B)** Gene Ontology Biological Process Over-representation analysis of BRD4i-mediated splicing events. Count refers to the number of alternatively spliced genes detected in the significantly over-represented pathway. **(C)** Transcript-level consequences of alternatively spliced genes as induced by RSV or BRD4 inhibition.

(IL6) cytokine (64, 65), a key cytokine in the innate immune response. In our dataset, we observe that BRD4i blocks this splicing event (50% reduction, P_{Adj} = 4.12e-11), maintaining *XBP1* mRNA in its longer, inactive form (Figure 2A). This coincides with an overall reduction in *XBP1* gene expression to dramatically reduce the abundance of *XBP1s* transcripts. We validate this result using q-RT-PCR primers targeting exon 4 of *XBP1s* (Figure 3C).

IFRD1, in contrast, is an under-studied, histone deacetylase-associated transcriptional regulator. Specifically, its function has been linked to the acetylation of NF-κB p65/RelA (66, 67) - a key activator of the innate response, which interacts with BRD4 when acetylated at lysine-310. In our model, we observe that BRD4i does not change overall gene expression of *IFRD1*. However, BRD4i does result in an alternative transcription start site located in the intron between exons 6 and 7. This excises exons 1-6, and results in a non-functional, non-coding transcript (P_{Adj} = 5.13e-10, Figure 2B). This result was confirmed by RT-PCR, using primers which span the intronic region and the canonical exons (Figures 3A, B).

In addition, we observe splicing events to the membrane-bound ATPase Phospholipid Transporting 11A (*ATP11A*), a member of the P4-ATPase Flippase complex, which is responsible for transporting a variety of phospholipids across the plasma membrane (68). Importantly, this complex has been linked to innate immunity *via* regulation of toll-like receptor (TLR) re-uptake into the plasma membrane from endocytic vesicles (69). Curiously, we observe that while BRD4i reduces the overall transcript-level abundance of ATP11A, it predominantly does so by ablating non-coding transcript variants (ATP11A-214: P_{Adj} = 0.012, ATP11A-215: P_{Adj} = 1e-45, ATP11A-217: P_{Adj} = 2e-7). Accordingly, the abundance of coding transcripts remains predominantly unchanged (Figure 2C). Due to the extreme heterogeneity in non-coding ATP11A transcripts, no RT-PCR assay could be designed to validate this event.

Protein-level validation of alternative splicing

To determine corresponding protein-level changes, we analyzed the proteome of hSAECs under identical biological conditions. Cells were pre-treated with ZL0454 or DMSO for 18 hours prior to infection with RSV at a multiplicity of infection (MOI) of 1. Control cells were left uninfected and untreated with ZL0454. 24 hours later, cells were harvested and processed for shotgun proteomic analysis by Data Independent Analysis - Parallel Acquisition Serial

10.3389/fimmu.2023.1212770

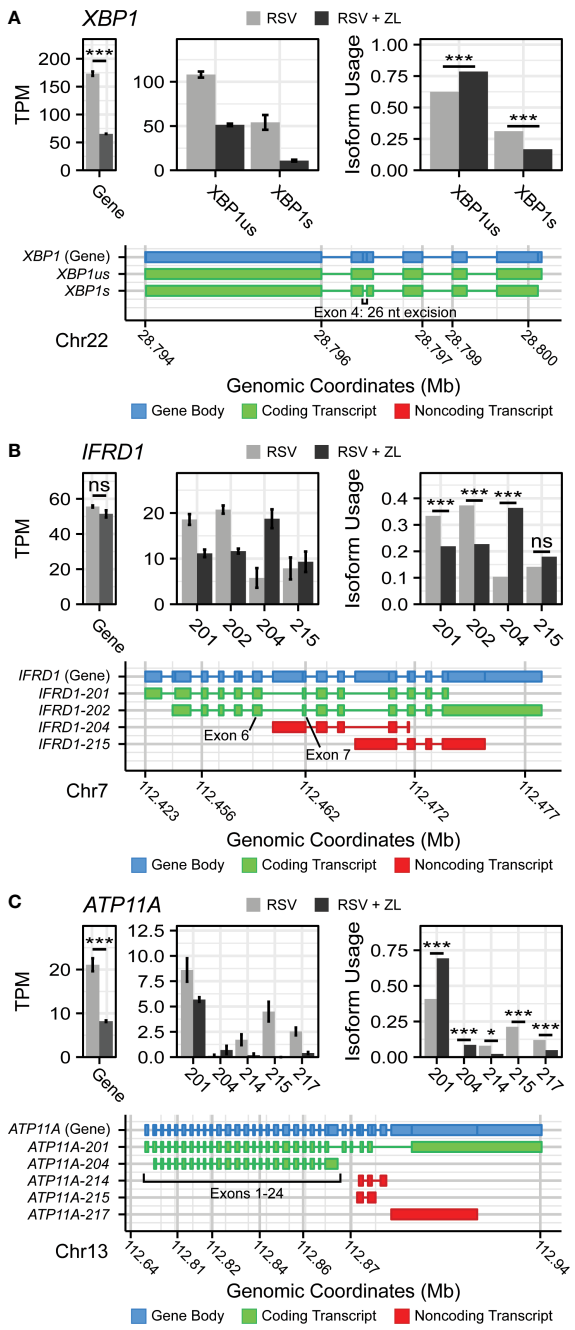

FIGURE 2
BRD4 inhibition induces isoform switching in key innate inflammation co-regulators. Transcript maps, RNA-seq quantitation in Transcripts per-Kilobase Million (TPM), and isoform usage of detected transcripts belonging to **(A)** XBP1, **(B)** IFRD1, and **(C)** ATP11A. Mapped transcripts are plotted in compressed genomic coordinates and color coded according to gene body and coding status. Barplots represents the mean of n=4 replicates per group. Error bars indicate the 95% confidence interval. Transcripts with less than 5% of total detected transcript abundance were omitted from this figure. * P_{Adj} < 0.05; *** P_{Adj} < 0.001.

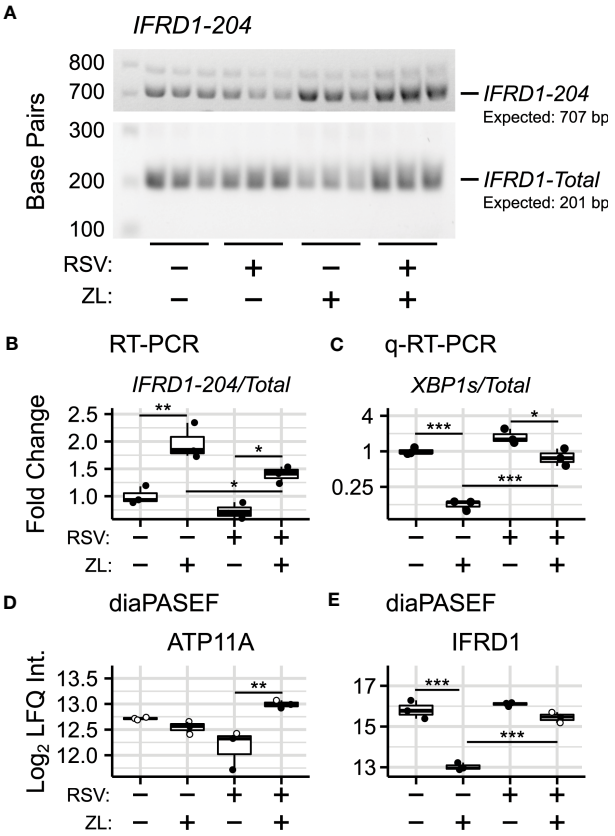

FIGURE 3
Validation of BRD4i-induced alternative splicing. **(A)** RT-PCR Amplification of IFRD1-204 and IFRD1-Total. **(B)** Gel Densitometry quantitation of IFRD1-204/IFRD1-Total Ratio. **(C)** q-RT-PCR quantitation of XBP1s/XBP1-Total Ratio. **(D, E)** Protein-level (diaPASEF) quantitation of ATP11A and IFRD1 abundance. Boxplots represent median and interquartile ranges of n=3 biological replicates per experimental group. Open circles represent imputed data points. *P_{Adj}< 0.05; **P_{Adj}< 0.01; ***P_{Adj}< 0.001.

Fragmentation (diaPASEF) (70). This enabled quantitation of ~8300 proteins, including 6 RSV proteins (1B, 1C, F, G, L, and P), with ~94.6% data completeness prior to filtering (Figure S1AD). Across 5 contrasts (RSV vs. Control; ZL0454 vs. Control; RSV + ZL0454 vs. Control; RSV + ZL0454 vs. RSV; RSV + ZL0454 vs. ZL0454), we observed 9332 statistically significant protein changes. Comparison of RSV-treated cells with ZL0454-treated cells was excluded from the differential abundance analysis to preserve statistical power. Reproducibility of biological replicates was high, as the lowest intra-group Pearson correlation score was 0.938, and the median coefficient of variation ranged from ~1-2% within groups (Figure S1BC). A full breakdown of differentially abundant proteins by contrast is available in Table S5. ~7500 genes had matched protein-level and transcript-level measurements. IFRD1 and ATP11A were among the proteins that were differentially abundant based on treatment with the BRD4 inhibitor (Figure 2D). XBP1/XBP1s was not detected by the proteomic analysis, most likely due to the extremely low abundance of this transcription factor.

In this analysis, we observed that the abundance of IFRD1 protein remains unchanged due to RSV-infection, but drops 8-fold when treated with the ZL0454 alone (Figure 3D; P_{Adj} = 0.00001). IFRD1 protein abundance is also slightly reduced by the inhibitor under the RSV condition (~38% reduction, P_{Adj} = 0.051), however, the abundance could not be reliably assayed in this group, as 2 of 3 values were missing in the proteomic dataset and were imputed for differential analysis (Table S6). This result is consistent with the

prediction from the alternative splicing analysis, in which BRD4i transitions the transcripts to a non-protein coding variant. ATP11A protein abundance, as predicted, remains unchanged when treated with the BRD4 inhibitor alone (Figure 3E). Interestingly, however, ATP11A abundance actually increases (~75%, P_{Adj} = 0.007) in the combined RSV + ZL0454 condition relative to RSV-treatment alone, despite a ~2.5-fold decrease at the total RNA level, and reverses a non-significant trend towards reduced ATP11A protein observed in RSV-treated cells. As the total abundance of the functional ATP11A transcript did not increase, this suggests that ATP11A is regulated by additional, post-translational mechanisms of gene regulation.

IFRD1-depletion reduces immediate-early innate inflammation

As IFRD1 function has been linked directly to RelA acetylation (66, 67), and RelA Lysine-310 acetylation (K310Ac) is required for BRD4-mediated inflammatory gene expression, we were interested in assaying the effects of IFRD1 depletion on the process of innate activation in airway epithelial cells. Pooled siRNA targeting IFRD1 was transfected into hSAECs, and peak knockdown efficiency was determined by western blot to occur after 72 hours (Figure S2).

IFRD1-depleted hSAECs were then stimulated with the Toll-like Receptor 3 (TLR3)-ligand, polyinosinic-polycytidilyic acid (polyIC), a synthetic viral replication intermediate that activates innate inflammation (71, 72). TLR3 signaling proceeds through BRD4:RelA-mediated transcriptional elongation, and accordingly, *IL6* was chosen as a marker of innate activation. In this knockdown model, we observed that expression of *IL6* was reduced ~2-fold (30 minutes: P_{Adj} = 0.0005; Overall: P_{Adj} = 4e-5) during early innate activation. (Figure 4A). However, this effect was no longer significant by 60 minutes post-stimulation, suggesting activation of compensatory pathways.

We also monitored the gene expression of the TNFα-induced Protein 3 *TNFAIP3* and NF-κB Inhibitor Alpha *NFKBIA* genes, which encode the A20 and IK$\beta\alpha$ proteins and are both NF-κB-dependent and highly-induced by innate activation (73). *NFKBIA* expression was similarly reduced by IFRD1 knockdown (60 minutes: P_{Adj} = 0.012; Overall: P_{Adj} = 0.02), but the effect did not ablate by 60 minutes post-stimulation (Figure 4B); *TNFAIP3* displayed only a non-significant trend (Figure 4C; P_{Adj} = 0.17) towards reduced gene expression. IFRD1 knockdown remained stable throughout the duration of the experiment (Figure S2).

Curious as to whether the inhibitory effects of IFRD1 knockdown behavior were a consequence of altered RelA-Acetylation, we immunoprecipitated RelA from unstimulated A549 alveolar epithelial cells and attempted to measure the K310Ac mark *via* immuno-blotting (Figure 4D). A549 cells have been extensively utilized for analysis of airway innate responses and maintain characteristics of type II alveolar cells (74, 75). To our surprise, we found that the abundance of the RelA K310Ac mark was not significantly affected by knockdown of IFRD1 (P_{Val} = 0.1). This result is inconsistent with previous works conducted in keritinocytes, in which RelA K310 acetylation was increased in response to IFRD1knockdown (67), and suggests that IFRD1 has cell-type or context-specific mechanisms of innate inflammatory regulation.

BRD4 regulates the abundance of Spliceosome components in airway epithelial cells

We next sought to determine mechanisms for spliced isoform changes, and accordingly examined the effects of BRD4i on the abundances of spliceosome components and splicing factors in the diaPASEF data. We noted that the abundance of Peptidylprolyl Isomerase H (PPIH) and Serine-and-Arginine-Rich Splicing Factors 1 and 9 (SRSF1/9) were reduced by ~50% (P_{Adj} = 0.026, 0.021, 0.026, respectively) in mock-infected cells treated with the ZL0454 BRD4 inhibitor. In addition, we noted smaller yet significant reductions to Peptidylprolyl Isomerase Like 4 (PPIL4, ~25% reduction, P_{Adj} = 0.047), and the core spliceosome subunit U2 Small Nuclear RNA Auxiliary Factor 2 (U2AF2, ~33% reduction, P_{Adj} = 0.03). Similar BRD4i-driven changes to PPIL4, SRSF1, and SRSF9 were also observed in the virus-treated condition (P_{Adj} = 0.052, 0.046, 0.016 respectively). Interestingly, the BRD4-driven reduction to U2AF2 appeared to be enhanced by virus infection (~63% reduction, P_{Adj} = 0.0015), despite RSV-infection alone having a non-significant effect on the protein's abundance (Figure 5A). U2AF2 is the spliceosome component responsible for binding intronic regions (76), and is considered essential for excision of most intronic regions (77, 78). Furthermore, U2AF2 knockdown, as well as knockdown of the Serine-and-Arginine-Rich Splicing Factors 1 and 9 (SRSF1/SRSF9) have been associated with exon skipping (79). Altogether, this argues that the reduction in abundance of core splicing factors contributes to the observed patterns of BRD4i-driven alternative splicing.

To evaluate the mechanism of BRD4-driven regulation of spliceosome components, we examined transcript-level changes to their abundance. In our dataset, no statistically significant differential isoform usage was detected for *PPIH*, *PPIL4*,*SRSF1*, or *SRSF9* (Table S4). *SNRPD1* and *U2AF2* exhibited minor isoform switching events which were not predicted to alter coding status. Overall transcript abundance was further validated using Q-RT-PCR assays measuring exon-exon junctions of selected protein-coding transcripts (Figure S3). q-RT-PCR analysis revealed corresponding, BRD4i-induced reductions to transcripts corresponding to exons 6-7 of *PPIH* (Mock: ~75% reduction, P_{Adj} = 0.001, RSV-Infected: P_{Adj} = 0.003), exons 1-2 of *PPIL4* (Mock: ~50% reduction, P_{Adj} = 0.003, RSV: ~50% reduction, P_{Adj} =~5e-4), exons 1-2 of *SNRPD1* (Mock: ~40% reduction, P_{Adj} = 3e-5, RSV: ~60% reduction, P_{Adj} =~3e-7) after ZL0454 treatment in both mock- and RSV-infected hSAECs (Figure 5B). *SRSF9* and *U2AF2* were also significantly reduced by ZL0454 treatment in RSV-infected cells (*SRSF9* Exons 1-2: ~50% reduction, P_{Adj} = 0.004, *U2AF2* Exons 9-10-11: ~50% reduction, P_{Adj} = 0.003), but not mock-infected cells (*SRSF9*: P_{Adj} = 0.26, *U2AF2*: P_{Adj} = 0.76). SRSF1, in contrast, did not demonstrate any transcript-level reduction due to BRD4 inhibition (Exons 2-3, Mock: P_{Adj} = 0.7, RSV: P_{Adj} = 0.45). Finally, we conducted Pearson Correlation analysis to compare the transcript- and protein-level abundances. Three spliceosome components demonstrated high

10.3389/fimmu.2023.1212770

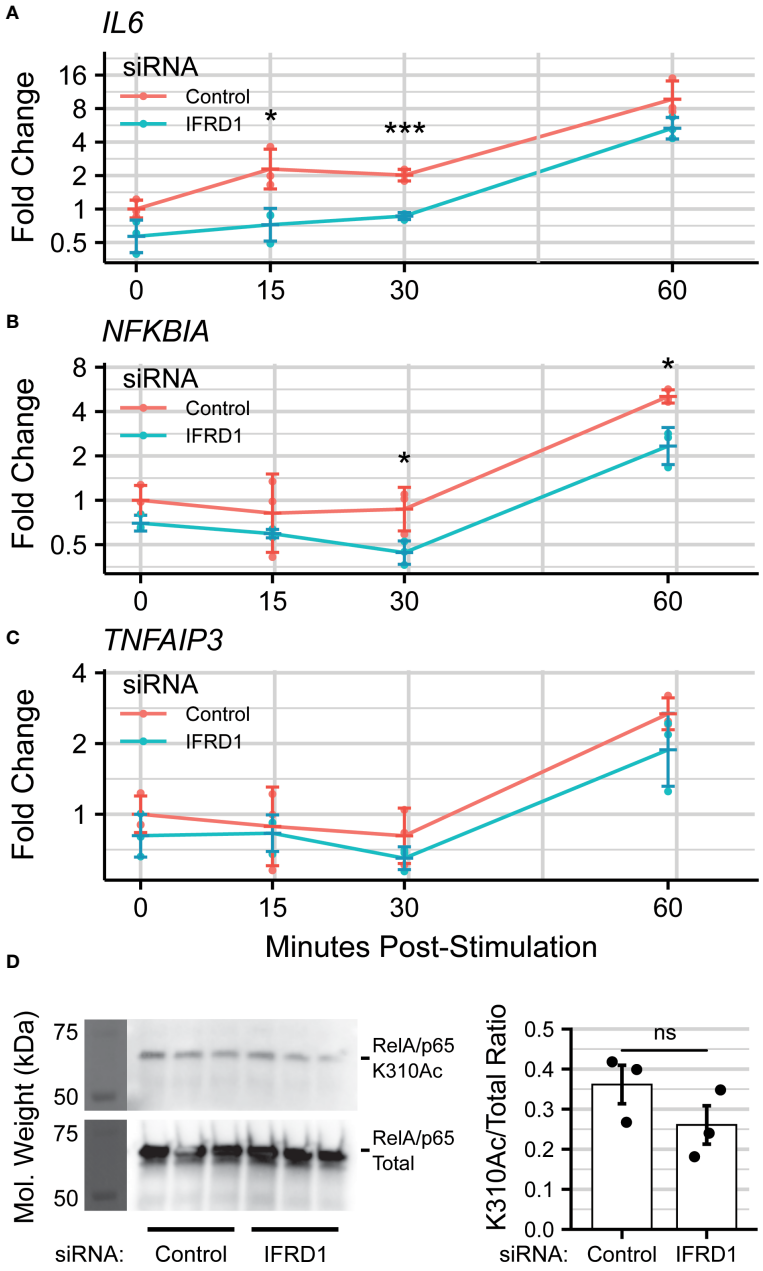

FIGURE 4
IFRD1 knockdown reduces NF- B-mediated expression in hSAECs. Timecourse q-RT-PCR experiment measuring **(A)** IL6, **(B)** (NFKBIA), and **(C)** (TNFAIP3) gene expression in hSAECs depleted of IFRD1. Data represents the geometric mean fold change ± standard error of n=3 biological replicates per experimental group. **(D)** Western blot and quantitation of RelA Lysine-310 Acetylation (K310Ac) as a function of IFRD1 knockdown by siRNA in A549 cells. Barplot represents the mean ± standard error of n=3 biological replicates. *P_{Adj}< 0.05; ***P_{Adj}< 0.001.

degrees of alignment with significant or near-significant correlation between q-RT-PCR and diaPASEF proteomic measurements (PPIL4: $R = 0.99, P_{Val} = 0.015$; SRSF9: $R = 0.92, P_{Val} = 0.075$; U2AF2: $R = 0.92, P_{Val} = 0.082$; Figure S4). However, the protein-level abundances of PPIH, SNRPD1, and SRSF1 were not well explained by the matching transcript-level abundances (PPIH: R = 0.62, $P_{V\ al}$ = 0.38; SNRPD1: R = 0.29, $P_{V\ al}$ = 0.29; SRSF1: R = 0.52, $P_{V\ al}$ = 0.48), signifying some degree of post-transcriptional regulation. Accordingly, we conclude that BRD4 regulates the abundance of spliceosome components and related splicing factors *via* both transcriptional and post-transcriptional mechanisms.

BRD4 regulates XBP1s splicing through transcriptional control of IRE1α

In addition to spliceosome-associated splicing factors, we were also able to quantify the effects of BRD4i on the endoplasmic reticulum (ER)-bound splicing factor Inositol-requiring Enzyme 1 α (IRE1α). IRE1α is an atypical protein kinase and endoribonuclease which is seated in the membrane of the ER, and uniquely splices *XBP1* transcripts into *XBP1s*. Interestingly, we observe that BRD4 inhibition blocks a ~75% increase in the abundance of IRE1α due to RSV infection ($P_{Adj} = 0.03$), which coincides with a reduction to

10.3389/fimmu.2023.1212770

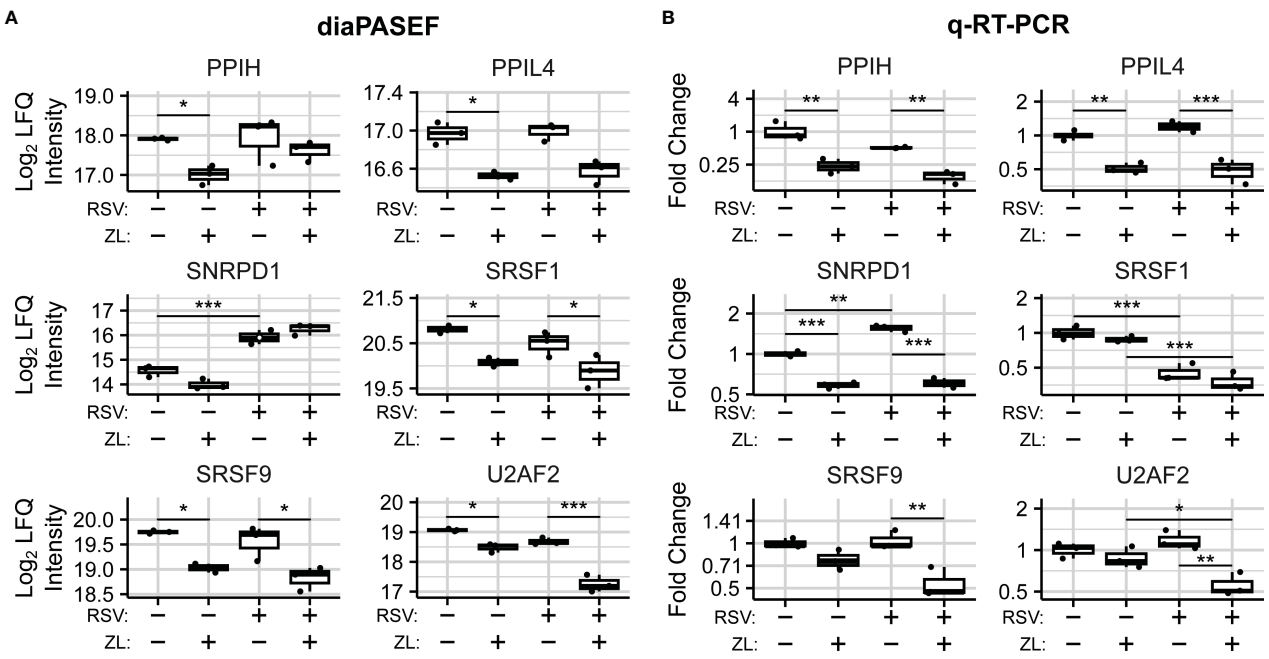

FIGURE 5
BRD4 regulates the transcript- and protein-level abundance of core splicing factors. **(A)** diaPASEF quantitation of core splicing factor protein abundance. Open circles indicate imputed data points. **(B)** q-RT-PCR quantitation of transcript-level splicing factor abundances. Boxplots represent median and interquartile range of n=3 biological replicates per experimental group. *P_{Adj}< 0.05; **P_{Adj}< 0.01; ***P_{Adj}< 0.001.

IRE1α gene expression in the same contrast (Figures 6A, B). The effect of ZL0454 alone was not statistically significant at the protein-level. However, we note that 2 of 3 biological replicates in this condition were imputed during differential abundance analysis, most likely indicating that they were below the limit of detection. Accordingly, we confirmed the effects of BRD4i on IRE1a in uninfected hSAECs by immunoblot, which demonstrated a ~4-fold reduction to the abundance of IRE1α (P_{Val} = 0.022, Figure 6C).

Given that BRD4 inhibition reduces both *XBP1* and *IRE1α* gene expression, these results suggested that BRD4 controls *XBP1* splicing through transcriptional control of *IRE1α*. To further investigate this hypothesis, we conducted chromatin immunoprecipitation (ChIP) assays to measure the abundance of BRD4 protein on the promoters of both genes in hSAECs infected with RSV and treated with ZL0454. This demonstrated a 4-8–fold enrichment of BRD4 on the promoters of these genes, however, the presence of BRD4 on these promoters was constitutive, and not responsive to RSV infection (Figures 6D, E). This suggests to us that BRD4 activates *IRE1α* and *XBP1* expression through stabilization or recruitment of additional transcriptional regulators on their proximal promoters.

Discussion

BRD4 mediates virus-induced innate airway inflammation

Respiratory Syncytial Virus (RSV) is a ubiquitous human pathogen for which no effective vaccine is approved, and is the single largest cause of pediatric hospitalizations in the United States (21). Replication of RSV or other airway viruses in the lungs induce airway epithelial cells to mount a robust innate inflammatory response to reduce viral replication and recruit cellular immune cells to the site of infection. This process represents a significant anti-viral barrier, and plays a major role in the resolution of the disease. The innate inflammatory pathway begins with pattern-recognition receptors (PRRs), such as Toll-like receptors on the cell surface and the retinoic-acid inducible gene (RIG-I) in the cytosol (6, 24), and largely proceeds through NF-κB and IRF transcription factors (27, 80, 81). These pathways converge on BRD4, which is an epigenetic scaffold that interacts with elements of the positive transcriptional elongation factor (pTEFb) (27). In this manner, BRD4 enables the transcriptional elongation and rapid expression of interferons, cytokines, and other genes with polymerases paused on their promoters (82). However, as innate inflammation is highly pleiotropic and stimulus-specific, and the exact mechanisms by which BRD4 facilitates transcription in a gene- and time-resolved manner have yet to be elucidated. BRD4 has also been shown to interact with components of the spliceosome and ribonuclear protein complexes (12, 13), suggesting a role in post-transcriptional regulation of gene products. These interactions have also been shown to be sensitive to BRD4 inhibition. In this work, we further demonstrate that BRD4 inhibition alters the splicing landscape of airway epithelial cells, resulting in altered abundances of proteins associated with the innate immune response and innate inflammation. These alternative splice events modulate innate signaling through the TLR3-NFκB signaling pathway and the unfolded protein response. Our data provide novel insights into the diverse anti-inflammatory actions of BRD4 inhibition.

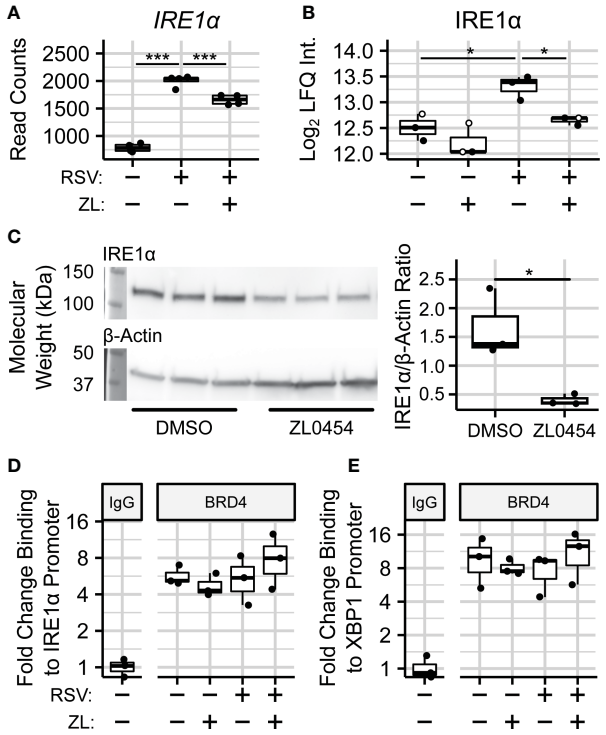

FIGURE 6
BRD4 controls the transcript- and protein-level abundance of IRE1α. **(A)** RNA sequencing read counts of summarized IRE1α transcripts. **(B)** Protein-level (diaPASEF) quantitation of IRE1α protein. Open circles represent imputed data points. **(C)** Immunoblot and Densitometric Quantitation of IRE1α from non-infected hSAECs treated with the BRD4 inhibitor ZL0454. **(D)** ChIP-PCR analysis of BRD4 binding to the IRE1α promoter. **(E)** ChIP-PCR analysis of BRD4 binding to the XBP1 promoter. Boxplots represent median and interquartile ranges of n=4 (RNA-seq) or n=3 (diaPASEF, Immunoblot, ChIP) biological replicates per experimental group. *P_{Adj}< 0.05; ***P_{Adj}< 0.001.

Pleiotropic activities of BRD4 in transcription-coupled RNA processing

Control of innate-inducible RNA Pol II-dependent gene expression is coordinated through a series of integrated steps including promoter initiation, elongation, RNA processing, termination and export (83). Although virtually all of these steps are regulated, immediate early genes in the innate response are thought to be primarily controlled at the level of transcriptional elongation. In uninfected cells, innate responsive genes are inactive, but found in open chromatin domains engaged by inactive/hypophosphorylated RNA Pol II (84, 85). Upon infection, NFκB repositions activated BRD4 complex. BRD4 kinase activity phosphorylates cyclin-dependent kinases and the carboxyterminal domain of RNA Pol II (86), transitioning it into an elongation-competent mode to express fully spliced inflammatory and antiviral genes.

Our study substantially extends this model by demonstrating that a subset of innate and stress-response genes undergo transcriptional elongation-coupled alternative splicing. These functional results are consistent with our earlier findings that BRD4 binds to the spliceosome in RSV infection, and is dependent on BD interaction with acetylate lysines. Future studies will be required to identify the spliceosome factors important for *IFRD1* and *ATP11A* isoform switching.

BRD4 inhibitors as a tool to study bromodomain biology

Bromodomain-and-extra-terminal-domain (BET) inhibitors have been used extensively over the last decade to probe bromodomain protein biology and disrupt related transcriptional activity (87, 88). Small molecule BET inhibitors function by competitively occupying the bromodomains of this family of proteins, and significant effort has been dedicated to developing protein-specific inhibitors for targeted inhibition and degradation of individual BET proteins. In the context of airway inflammation, BET inhibition has been shown to block BRD4-mediated inflammatory activation and induced expression of cytokines and interferons (31). Furthermore, BET inhibition blocks airway fibrosis and remodeling that proceeds through the epithelial-to-mesenchymal transition (EMT).

Classically, bromodomain inhibitors suffer from low specificity and high toxicity (88). To address this issue and specifically probe BRD4, we use the highly specific and selective BRD4 inhibitor ZL0454, previously developed and used by our research group (30), using structure-based drug design to identify acetyl-lysine blocking chemistries. ZL0454 shows high selectivity for both bromodomains of BRD4, and displaces acetylated lysine side chains from the bromodomain (BD)-1 and -2 of BRD4 with an IC_{50} of approximately 50 nM as determined by time-resolved fluorescence resonance energy transfer (TR-FRET) assays. Furthermore, ZL0454 binds to BRD4 16-20 times stronger than the bromodomains of the closely related BRD2, BRD3, and BRDT. Compared to other notable BET inhibitors, ZL0454 also does not produce detectable toxicity in cell culture or *in vivo*. Finally, ZL0454 has been shown to reduce recruitment of interactors to the BRD4 complex, including key members of the spliceosome (12). These traits make ZL0454 an ideal probe to study the role of BRD4 at the confluence of alternative splicing and innate inflammation.

BRD4 regulates alternative splicing of key innate inflammation co-regulators

Recent works have demonstrated that BRD4 interacts with components of the spliceosome, and that these interactions can mediate alternative splicing in the context of T cell acute lymphoblastic leukemia (13). Furthermore, BRD4:Spliceosome interactions have been shown to be dynamic in the context of airway viral infection, and sensitive to bromodomain inhibition (12). In this work, we further investigate BRD4's role in alternative splicing in the context of airway viral infection using a highly selective BRD4-specific inhibitor, ZL0454. In our data, treatment with ZL0454 resulted in detectable splicing events in 822 genes. Gene Ontology analysis identified only four significantly enriched

pathways among these genes, suggesting that BRD4's impact on alternative splicing in the airway epithelium is not biased for individual biological pathways, but rather widespread throughout the transcriptome. Nevertheless, observed splicing changes were significantly enriched for intron retention and extended Open Reading Frames, suggesting a coordinated mechanism of action. Among these alternatively spliced genes, we highlight three notable genes associated with innate inflammation, cytokine activation, and fibrosis: X-Box Binding Protein 1 (XBP1), ATPase Phospholipid Transporting 11A (ATP11A), and Interferon-related Developmental Regulator 1 (IFRD1).

XBP1 is a transcription factor essential to the activation of the immune response and the unfolded protein response (62, 65). In the context of endoplasmic reticulum (ER) stress, the dual-function protein kinase/endoribonuclease IRE1α splices out a 26-nucleotide sequence from full-length XBP1 mRNA (63). The resulting frame-shift enables translation of the active XBP1s protein, which translocates to the nucleus and serves as a potent transcriptional activator. In viral-induced innate inflammation, XBP1s directly binds the IL6 promoter and regulates expression of the key cytokine (65). Furthermore, XBP1s has been implicated as a driver of fibrotic disease (89–91). Our results further demonstrate that BRD4 regulates both the gene expression and alternative splicing of XBP1s, with IRE1α similarly effected, and provides a direct link between BRD4 and XBP1-mediated cytokine activation. However, the mechanism of this behavior, and the nature of its relationship with IRE1α remain to be fully elucidated. As BRD4 has been shown to interact with numerous transcription factors and chromatin remodeling factors (12), we propose that BRD4 may be serving as a scaffold for transcriptional co-regulators that directly control IRE1α and XBP1 gene expression. Future works that evaluate BRD4's role in stabilizing such interactions at these gene bodies will be invaluable for understanding this mechanism of innate immune regulation.

ATP11A in contrast, is a membrane bound flippase - a class of enzymes responsible for "flipping" phospholipids across surfaces of the cellular plasma membrane (68). In particular, ATP11A is a member of the P4 ATPase Flippase complex, which has been directly linked to the recycling of Toll-like Receptor 4 (TLR4) back into the plasma membrane (69). In human macrophages, knockdown of ATP11A induced hypersensitivity to lipopolysaccharide (LPS), due to an increase in membrane-associated TLR4. In our data set, we observed that BRD4i specifically reduces the expression of non-coding transcripts, while leaving protein-coding transcripts largely untouched, and in fact increased the abundance of ATP11A protein. This discrepancy likely signals the existence of additional layers of regulation, such as proteolytic degradation, but suggests that BRD4 may influence the activity of upstream components of the NF-κB and innate immune signaling cascade. Additional studies to measure the cellular localization of TLR4 and other Toll-like receptors as a consequence of BRD4 inhibition will likely be illuminating.

Finally, we remark on IFRD1, which is especially interesting given its close relationship to NF-κB p65/RelA. Studies in muscle tissue and keratinocytes have demonstrated that IFRD1 associates with histone deacetylases 3 and 4 (HDAC3/HDAC4) to attenuate the acetylation state of RelA (66, 92). As RelA acetylation is a key marker of innate inflammation and is required for its interaction with BRD4 and the pTEFb complex (6, 27), this led to an expected decrease in the abundance of pro-inflammatory cytokines. IFRD1 overexpression in mice and human bronchiole epithelioid cells also reduced inflammation (93). However, neutrophils from IFRD1-knockout mice demonstrate a reduced inflammatory phenotype, and our data suggests that IFRD1 in small airway epithelial cells actually blunts basal inflammation (94). These findings suggest cell-type and/or stimulus-dependent roles for IFRD1, and additional studies which directly examine IFRD1's interactions with HDACs may be valuable to precisely qualify IFRD1's role in airway inflammation. In addition, there is currently no high-sensitivity method to examine site-specific RelA acetylation, with the exception of the K310Ac mark (95). Novel, mass spectrometry-based analytical methods may enable precise quantitation of IFRD1's impact on RelA acetylation, stratified by airway cell-type and stimulus.

BRD4 regulates the abundance of interacting splicing factors in airway epithelial cells

In the process of measuring protein-level splicing consequences, we discovered that BRD4 regulates the protein-level abundance of several splicing factors. In particular, we highlight the core splicing factor, U2AF subunit 2 (U2AF2), which is known to complex with RNA polymerase II (96), coupling alternative splicing to transcription. U2AF2 has also been found to interact directly with BRD4 (13), and is dynamically recruited by RSV-infection (12), suggesting a 3-way association between innate-activated transcriptional machinery and the spliceosome in the context of the airway epithelium. Given the close interactions between these proteins, this finding initially suggested a post-translational mechanism for abundance regulation. However, targeted q-RT-PCR assays indicate that a considerable degree of this regulation occurs at the transcript-level. Curiously, this result is not mirrored in other studies of BRD4-regulated gene expression (13, 28, 97). The mechanism for this discrepancy is unclear, and may stem from differences in biological and experimental models used to explore BRD4 inhibition and deficiency. However, this result agrees with our group's previous finding - that BRD4 transcriptionally regulates the abundance of its interacting co-activators - and emphasizes the multi-faceted, key role that BRD4 takes in systems biology (28).

Challenges in multi-omic analysis

Short-read RNA-sequencing is a widely applied technique for profiling changes to gene-product abundance in biological samples (98, 99). When transcripts are summarized to gene-level statistics, RNA-seq is highly accurate and can achieve nearly complete genome coverage. However, it is well-established that transcript-level abundance and relative abundance changes do not correlate perfectly to protein-level abundance (100–102). This owes to the multiple post-transcriptional mechanisms of abundance control, including alternative mRNA splicing and post-translational degradation. In this

study, we address this limitation by utilizing a splice-aware analysis pipeline to measure transcript-level abundances, and high-sensitivity, liquid-chromatography - Data-Independent Analysis Parallel Acquisition - Serial Fragmentation Tandem Mass Spectrometry (LC-diaPASEF-MS/MS) to provide protein-level validation.

This integrated analysis offered combined coverage of ~7500 genes, however, it is worth noting that the quantifiable transcriptome of hSAECs includes nearly 20,000 genes. Many proteins, such as XBP1, are present at such low abundances that they cannot currently be quantified by our method. Significant improvements in proteomics technologies, particularly focused towards sensitivity and dynamic range, will be essential for comprehensive multi-omic quantitation of gene products. Furthermore, both short-read RNA-sequencing and shotgun proteomics use short, fragmented sequences as proxy for whole-transcript/protein abundance (99, 103). This approach, while robust for whole-protein quantitation, cannot comprehensively identify and quantify all possible transcript variants and proteoforms (104). Recent advances in long-read nano-pore sequencing (105, 106), and future advances in intact protein analysis (107–109) may allow for a truly comprehensive multi-omic analysis pipeline.

Conclusion

In summary, we utilize a multi-omics approach integrating state-of-the-art proteomics and transcriptomic profiling, in concert with BRD4-specific small molecule bromodomain inhibitors, to identify BRD4-mediated alternative splicing in the context of the human airway epithelium. Further interrogating the results, we link BRD4-mediated alternative splicing to key regulators of innate activation, including X-box Binding Protein 1 (XBP1), ATPase Phospholipid Transporting 11A (ATP11A), and Interferon-related Developmental Regulator 1 (IFRD1). Finally, functional analysis of IFRD1 knockdown in this cell line revealed unexpected negative regulation of cytokine expression. These results directly clarify mechanisms of BRD4-mediated innate inflammation.

Data availability statement

This paper analyzes existing, publicly available data, available at the following repository and accession number: https://www.ncbi.nlm.nih.gov/geo (GSE179353). Raw mass spectrometry data have been deposited to the ProteomeXchange Consortium via the PRIDE (59) partner repository (Accession: PXD039212), and is publicly available as of the date of publication. Original qPCR data, and blot and gel images have been deposited at the Dryad repository (doi:10.5061/dryad.j0zpc86jr).

Author contributions

MM: Conceptualization, Methodology, Software, Validation, Formal Analysis, Investigation, Writing - Original Draft, Visualization. YF: Validation, Investigation, Writing - Review and Editing. RG: Validation, Investigation, Writing - Review and Editing. XX: Resources, Writing - Review and Editing. DR: Resources, Writing - Review and Editing, Supervision. YL: Resources, Writing - Review and Editing. JZ: Resources, Writing - Review and Editing. YG: Resources, Supervision, Writing - Review and Editing, Project Administration. AB: Conceptualization, Resources, Writing - Review and Editing, Supervision, Project Administration, Funding Acquisition. All authors contributed to the article and approved the submitted version.

Funding

This work was partially supported by NIH grants AI062885 (AB) and NCATS UL1TR002373 (AB). DSR would like to acknowledge support from the American Heart Association Predoctoral Fellowship Grant No. 832615/David S. Roberts/2021. JZ is also partly supported by the John D. Stobo, M.D. Distinguished Chair Endowment Fund. The funders had no role in the design of the study; in the collection, analyses, or interpretation of data; in the writing of the manuscript, or in the decision to publish the results.

Acknowledgments

The authors acknowledge the UW-Madison Human Proteomics Program Mass Spectrometry Facility (initially funded by the Wisconsin partnership funds) for support in obtaining mass spectrometry data and NIH S10OD018475 for the acquisition of ultra-high resolution mass spectrometer for biomedical research. We also thank Bruker for providing the timsTOF Pro mass spectrometer that was used in the study for the collection of all mass spectrometry data.

Conflict of interest

The University of Wisconsin—Madison holds a patent for the use of Azo in proteomics applications. JZ and AB hold a patent on ZL0454 chemistry.

The remaining authors declare that the research was conducted in the absence of any commercial or financial relationships that could be construed as a potential conflict of interest.

Publisher's note

Supplementary material

The Supplementary Material for this article can be found online at: https://www.frontiersin.org/articles/10.3389/fimmu.2023.1212770/full#supplementary-material

References

1. Xu Y, Vakoc CR. Brd4 is on the move during inflammation. *Trends Cell Biol* (2014) 24:615–6. doi: 10.1016/j.tcb.2014.09.005

2. Hajmirza A, Emadali A, Gauthier A, Casasnovas O, Gressin R, Callanan MB. BET family protein BRD4: an emerging actor in NFκB signaling in inflammation and cancer. *Biomedicines* (2018) 6. doi: 10.3390/biomedicines6010016

3. Donati B, Lorenzini E, Ciarrocchi A. BRD4 and cancer: going beyond transcriptional regulation. *Mol Cancer* (2018) 17:164. doi: 10.1186/s12943-018-0915-9

4. Zhu W, Wu RD, Lv YG, Liu YM, Huang H, Xu JQ. BRD4 blockage alleviates pathological cardiac hypertrophy through the suppression of fibrosis and inflammation *via* reducing ROS generation. *BioMed Pharmacother* (2020) 121:109368. doi: 10.1016/j.biopha.2019.109368

5. Ding N, Hah N, Yu RT, Sherman MH, Benner C, Leblanc M, et al. BRD4 is a novel therapeutic target for liver fibrosis. *Proc Natl Acad Sci U.S.A.* (2015) 112:15713–8. doi: 10.1073/pnas.1522163112

6. Tian B, Yang J, Zhao Y, Ivanciuc T, Sun H, Garofalo RP, et al. BRD4 couples NF-κB/RelA with airway inflammation and the IRF-RIG-I amplification loop in respiratory syncytial virus infection. *J Virol* (2017) 91:e00007–17. doi: 10.1128/JVI.00007-17

7. Tian B, Zhao Y, Sun H, Zhang Y, Yang J, Brasier AR. BRD4 mediates NF-κBdependent epithelial-mesenchymal transition and pulmonary fibrosis **via** transcriptional elongation. *Am J Physiology-Lung Cell Mol Physiol* (2016) 311:L1183–201. doi: 10.1152/ajplung.00224.2016

8. Bergeron C, Tulic MK, Hamid Q. Airway remodelling in asthma: from benchside to clinical practice. *Can Respir J J Can Thorac Soc* (2010) 17:e85–93. doi: 10.1155/2010/318029

9. Dey A, Chitsaz F, Abbasi A, Misteli T, Ozato K. The double bromodomain protein Brd4 binds to acetylated chromatin during interphase and mitosis. *Proc Natl Acad Sci U.S.A.* (2003) 100:8758–63. doi: 10.1073/pnas.1433065100

10. Jung M, Philpott M, M¨uller S, Schulze J, Badock V, Ebersp¨acher U, et al. Affinity map of bromodomain protein 4 BRD4. interactions with the histone H4 tail and the small molecule inhibitor JQ1. *J Biol Chem* (2014) 289:9304–19. doi: 10.1074/jbc.M113.523019

11. Devaiah BN, Singer DS. Two faces of brd4: mitotic bookmark and transcriptional lynchpin. *Transcription* (2013) 4:13–7. doi: 10.4161/trns.22542

12. Mann M, Roberts DS, Zhu Y, Li Y, Zhou J, Ge Y, et al. Discovery of RSV-induced BRD4 protein interactions using native immunoprecipitation and parallel accumulation–serial fragmentation PASEF. *Mass Spectrometry Viruses* (2021) 13:454. doi: 10.3390/v13030454

13. Uppal S, Gegonne A, Chen Q, Thompson PS, Cheng D, Mu J, et al. The bromodomain protein 4 contributes to the regulation of alternative splicing. *Cell Rep* (2019) 29:2450–2460.e5. doi: 10.1016/j.celrep.2019.10.066

14. Wilkinson ME, Charenton C, Nagai K. RNA Splicing by the spliceosome. *Annu Rev Biochem* (2020) 89:359–88. doi: 10.1146/annurev-biochem-091719-064225

15. Will CL, Lührmann R. Spliceosome structure and function. *Cold Spring Harbor Perspect Biol* (2011) 3. doi: 10.1101/cshperspect.a003707

16. Matera AG, Wang Z. A day in the life of the spliceosome. *Nat Rev Mol Cell Biol* (2014) 15:108. doi: 10.1038/nrm3742

17. Twyffels L, Gueydan C, Kruys V. Shuttling SR proteins: more than splicing factors. *FEBS J* (2011) 278:3246–55. doi: 10.1111/j.1742-4658.2011.08274.x

18. M¨uller-McNicoll M, Botti V, de Jesus Domingues AM, Brandl H, Schwich OD, Steiner MC, et al. SR proteins are NXF1 adaptors that link alternative RNA processing to mRNA export. *Genes Dev* (2016) 30:553–66. doi: 10.1101/gad.276477.115

19. WANG Y, LIU J, HUANG B, XU Y-M, LI J, HUANG L-F, et al. Mechanism of alternative splicing and its regulation. *Biomed Rep* (2015) 3:152–8. doi: 10.3892/br.2014.407

20. Eiland LS. Respiratory syncytial virus: diagnosis, treatment and prevention. *J Pediatr Pharmacol Ther* (2009) 14:75–85. doi: 10.5863/1551-6776-14.2.75

21. Group, P. E. R. f. C. H. P. S. Causes of severe pneumonia requiring hospital admission in children without HIV infection from Africa and Asia: the PERCH multi-country case-control study. *Lancet* (2019) 394:757–79. doi: 10.1016/S0140-6736(19)30721-4

22. Abbasi J. "This is our COVID"–what physicians need to know about the pediatric RSV surge. *JAMA* (2022) 328:2096–8. doi: 10.1001/jama.2022.21638

23. Zhang Y, Luxon BA, Casola A, Garofalo RP, Jamaluddin M, Brasier AR. Expression of respiratory syncytial virus-induced chemokine gene networks in lower airway epithelial cells revealed by cDNA microarrays. *J Virol* (2001) 75:9044–58. doi: 10.1128/JVI.75.19.9044-9058.2001

24. Liu P, Jamaluddin M, Li K, Garofalo RP, Casola A, Brasier AR. Retinoic acid-inducible gene I mediates early antiviral response and toll-like receptor 3 expression in respiratory syncytial virus-infected airway epithelial cells. *J Virol* (2007) 81:1401–11. doi: 10.1128/JVI.01740-06

25. Zhao Y, Jamaluddin M, Zhang Y, Sun H, Ivanciuc T, Garofalo RP, et al. Systematic analysis of cell-type differences in the epithelial secretome reveals insights into the pathogenesis of respiratory syncytial virus-induced lower respiratory tract infections. *J Immunol* (2017) 198:3345–64. doi: 10.4049/jimmunol.1601291

26. Hosakote YM, Brasier AR, Casola A, Garofalo RP, Kurosky A. Respiratory syncytial virus infection triggers epithelial HMGB1 release as a damage-associated molecular pattern promoting a monocytic inflammatory response. *J Virol* (2016) 90:9618–31. doi: 10.1128/JVI.01279-16

27. Brasier AR, Tian B, Jamaluddin M, Kalita MK, Garofalo RP, Lu M. RelA Ser276 phosphorylation-coupled Lys310 acetylation controls transcriptional elongation of inflammatory cytokines in respiratory syncytial virus infection. *J Virol* (2011) 85:11752–69. doi: 10.1128/JVI.05360-11

28. Xu X, Mann M, Qiao D, Li Y, Zhou J, Brasier AR. Bromodomain containing protein 4 BRD4. regulates expression of its interacting coactivators in the innate response to respiratory syncytial virus. *Front Mol Biosci* (2021) 8:728661. doi: 10.3389/fmolb.2021.728661

29. Liu W, Sun Y, Qiu X, Meng C, Song C, Tan L, et al. Genome-wide analysis of alternative splicing during host-virus interactions in chicken. *Viruses* (2021) 13:2409. doi: 10.3390/v13122409

30. Liu Z, Tian B, Chen H, Wang P, Brasier AR, Zhou J. Discovery of potent and selective BRD4 inhibitors capable of blocking TLR3-induced acute airway inflammation. *Eur J Medicinal Chem* (2018) 151:450–61. doi: 10.1016/j.ejmech.2018.04.006

31. Tian B, Liu Z, Litvinov J, Maroto R, Jamaluddin M, Rytting E, et al. Efficacy of novel highly specific bromodomain-containing protein 4 inhibitors in innate inflammation-driven airway remodeling. *Am J Respir Cell Mol Biol* (2019) 60:68–83. doi: 10.1165/rcmb.2017-0445OC

32. Brown KA, Chen B, Guardado-Alvarez TM, Lin Z, Hwang L, Ayaz-Guner S, et al. A photocleavable surfactant for top-down proteomics. *Nat Methods* (2019) 16:417–20. doi: 10.1038/s41592-019-0391-1

33. Brown KA, Tucholski T, Eken C, Knott S, Zhu Y, Jin S, et al. High throughput proteomics enabled by a photocleavable surfactant. *Angewandte Chemie Int Edition* (2020) 59:8406–10. doi: 10.1002/anie.201915374

34. Tian B, Yang J, Zhao Y, Ivanciuc T, Sun H, Wakamiya M, et al. Central role of the NF-κB pathway in the Scgb1a1-expressing epithe-lium in mediating respiratory syncytial virus-induced airway inflammation. *J Virol* (2018) 92:e00441–18. doi: 10.1128/JVI.00441-18

35. Garofalo R, Sabry M, Jamaluddin M, Yu RK, Casola A, Ogra PL, et al. Transcriptional activation of the interleukin-8 gene by respiratory syncytial virus infection in alveolar epithelial cells: nuclear translocation of the RelA transcription factor as a mechanism producing airway mucosal inflammation. *J Virol* (1996) 70:8773–81. doi: 10.1128/jvi.70.12.8773-8781.1996

36. Ueba O. Respiratory syncytial virus. i. concentration and purification of the infectious virus. *Acta Med Okayama* (1978) 32:265–72.

37. Xu X, Qiao D, Mann M, Garofalo RP, Brasier AR. Respiratory syncytial virus infection induces chromatin remodeling to activate growth factor and extracellular matrix secretion pathways. *Viruses* (2020) 12. doi: 10.3390/v12080804

38. Ramirez RD, Sheridan S, Girard L, Sato M, Kim Y, Pollack J, et al. Immortalization of human bronchial epithelial cells in the absence of viral oncoproteins. *Cancer Res* (2004) 64:9027–34. doi: 10.1158/0008-5472.CAN-04-3703

39. Ijaz T, Pazdrak K, Kalita M, Konig R, Choudhary S, Tian B, et al. Systems biology approaches to understanding epithelial mesenchymal transition EMT. **@ in** mucosal remodeling and signaling in asthma. *World Allergy Organ J* (2014) 7:13. doi: 10.1186/1939-4551-7-13

40. Schindelin J, Arganda-Carreras I, Frise E, Kaynig V, Longair M, Pietzsch T, et al. Fiji - an open source platform for biological image analysis. *Nat Methods* (2012) 9:676–82. doi: 10.1038/nmeth.2019

41. Tian B, Yang J, Brasier AR. Two-step crosslinking for analysis of protein-chromatin interactions. *Methods Mol Biol Clifton N.J* (2012) 809:105–20. doi: 10.1007/978-1-61779-376-9_7

42. Vitting-Seerup K, Sandelin A. IsoformSwitchAnalyzeR: analysis of changes in genome-wide patterns of alternative splicing and its functional consequences. *Bioinf Oxford England* (2019) 35:4469–71. doi: 10.1093/bioinformatics/btz247

43. Frankish A, Diekhans M, Jungreis I, Lagarde J, Loveland JE, Mudge JM, et al. GENCODE 2021. *Nucleic Acids Res* (2020) 49:D916–23. doi: 10.1093/nar/gkaa1087

44. Wang L, Park HJ, Dasari S, Wang S, Kocher J-P, Li W. CPAT: coding-potential assessment tool using an alignment-free logistic regression model. *Nucleic Acids Res* (2013) 41:e74. doi: 10.1093/nar/gkt006

45. Mistry J, Chuguransky S, Williams L, Qureshi M, Salazar G, Sonnhammer ELL, et al. Pfam: the protein families database in 2021. *Nucleic Acids Res* (2020) 49:D412–D419. doi: 10.1093/nar/gkaa913

46. Almagro Armenteros JJ, Tsirigos KD, Sønderby CK, Petersen TN, Winther O, Brunak S, et al. SignalP 5.0 improves signal peptide predictions using deep neural networks. *Nat Biotechnol* (2019) 37:420–423. doi: 10.1038/s41587-019-0036-z

47. Erd˝os G, Doszt´anyi Z. Analyzing protein disorder with IUPred2A. *Curr Protoc Bioinf* (2020) 70:e99. doi: 10.1002/cpbi.99

48. Thomas PD, Campbell MJ, Kejariwal A, Mi H, Karlak B, Daverman R, et al. PANTHER: a library of protein families and subfamilies indexed by function. *Genome Res* (2003) 13:2129–41. doi: 10.1101/gr.772403

49. Thomas PD, Kejariwal A, Guo N, Mi H, Campbell MJ, Muruganu-jan A, et al. Applications for protein sequence–function evolution data: mRNA/protein expression analysis and coding SNP scoring tools. *Nucleic Acids Res* (2006) 34:W645–50. doi: 10.1093/nar/gkl229

50. Wickham H. *ggplot2: elegant graphics for data analysis*. New York: Springer-Verlag (2016).

51. Kassambara A. *Ggpubr: 'ggplot2' based publication ready plots* (2020). Available at: https://CRAN.R-project.org/package=ggpubr.

52. R Core Team. *R: a language and environment for statistical computing*. Vienna, Austria: R Foundation for Statistical Computing (2022).

53. Demichev V, Messner CB, Vernardis SI, Lilley KS, Ralser M. DIA-NN: neural networks and interference correction enable deep proteome coverage in high throughput. *Nat Methods* (2020) 17:41–4. doi: 10.1038/s41592-019-0638-x

54. The UniProt Consortium. UniProt: the universal protein knowledgebase in 2023. *Nucleic Acids Res* (2022) 51:gkac1052. doi: 10.1093/nar/gkac1052

55. Wieczorek S, Combes F, Lazar C, Giai Gianetto Q, Gatto L, Dorffer A, et al. Software to perform statistical analyses in quantitative discovery proteomics. *Bioinformatics* (2017) 33:135–6. doi: 10.1093/bioinformatics/btw580

56. Zhang X, Smits AH, van Tilburg GB, Ovaa H, Huber W, Vermeulen M. Proteome-wide identification of ubiquitin interactions using UbIA-MS. *Nat Protoc* (2018) 13:530–50. doi: 10.1038/nprot.2017.147

57. Ignatiadis N, Klaus B, Zaugg JB, Huber W. Data-driven hypothesis weighting increases detection power in genome-scale multiple testing. *Nat Methods* (2016) 13:577–80. doi: 10.1038/nmeth.3885

58. Pino LK, Searle BC, Bollinger JG, Nunn B, MacLean B, MacCoss MJ. The skyline ecosystem: informatics for quantitative mass spectrometry proteomics. *Mass Spectrometry Rev* (2020) 39:229–44. doi: 10.1002/mas.21540

59. Perez-Riverol Y, Csordas A, Bai J, Bernal-Llinares M, Hewapathirana S, Kundu DJ, et al. The PRIDE database and related tools and resources in 2019: improving support for quantification data. *Nucleic Acids Res* (2019) 47:D442–50. doi: 10.1093/nar/gky1106

60. Tian B, Liu Z, Yang J, Sun H, Zhao Y, Wakamiya M, et al. Selective antagonists of the bronchiolar epithelial NF-κB-Bromodomain-Containing protein 4 pathway in viral-induced airway inflammation. *Cell Rep* (2018) 23:1138–51. doi: 10.1016/j.celrep.2018.03.106

61. Hu J, Tian C-Q, Damaneh MS, Li Y, Cao D, Lv K, et al. Structure-based discovery and development of a series of potent and selective bromodomain and extra-terminal protein inhibitors. *J Med Chem* (2019) 62:8642–63. doi: 10.1021/acs.jmedchem.9b01094

62. Yoshida H. Unconventional splicing of XBP-1 mRNA in the unfolded protein response. *Antioxidants Redox Signaling* (2007) 9:2323–33. doi: 10.1089/ars.2007.1800

63. Yoshida H, Matsui T, Yamamoto A, Okada T, Mori K. XBP1 mRNA is induced by ATF6 and spliced by IRE1 in response to ER stress to produce a highly active transcription factor. *Cell* (2001) 107:881–91. doi: 10.1016/S0092-8674(01)00611-0

64. Fang P, Xiang L, Huang S, Jin L, Zhou G, Zhuge L, et al. IRE1α-XBP1 signaling pathway regulates IL-6 expression and promotes progression of hepatocellular carcinoma. *Oncol Lett* (2018) 16:4729–4736. doi: 10.3892/ol.2018.9176

65. Chen C, Zhang X. IRE1α-XBP1 pathway promotes melanoma progression by regulating IL-6/STAT3 signaling. *J Trans Med* (2017) 15:42. doi: 10.1186/s12967-017-1147-2

66. Micheli L, Leonardi L, Conti F, Maresca G, Colazingari S, Mattei E, et al. PC4/Tis7/IFRD1 stimulates skeletal muscle regeneration and is involved in myoblast differentiation as a regulator of MyoD and NF-κB. *J Biol Chem* (2011) 286:5691–707. doi: 10.1074/jbc.M110.162842

67. Tummers B, Goedemans R, Pelascini LPL, Jordanova ES, van Esch EMG, Meyers C, et al. The interferonrelated developmental regulator 1 is used by human papillomavirus to suppress NFκB activation. *Nat Commun* (2015) 6:6537. doi: 10.1038/ncomms7537

68. van der Mark VA, Oude Elferink RP, Paulusma CC. P4 ATPases: flippases in health and disease. *Int J Mol Sci* (2013) 14:7897–922. doi: 10.3390/ijms14047897

69. van der Mark VA, Ghiboub M, Marsman C, Zhao J, van Dijk R, Hiralall JK, et al. Phospholipid flippases attenuate LPS-induced TLR4 signaling by mediating endocytic retrieval of toll-like receptor 4. *Cell Mol Life Sci* (2017) 74:715–30. doi: 10.1007/s00018-016-2360-5

70. Meier F, Brunner A-D, Frank M, Ha A, Bludau I, Voytik E, et al. diaPASEF: parallel accumulation–serial fragmentation combined with data-independent acquisition. *Nat Methods* (2020) 17:1229–36. doi: 10.1038/s41592-020-00998-0

71. Lever AR, Park H, Mulhern TJ, Jackson GR, Comolli JC, Borenstein JT, et al. Comprehensive evaluation of polyI:C. induced inflammatory response in an airway epithelial model. *Physiol Rep* (2015) 3. doi: 10.14814/phy2.12334

72. Aeffner F, Traylor ZP, Yu ENZ, Davis IC. Double-stranded RNA induces similar pulmonary dysfunction to respiratory syncytial virus in BALB/c mice. American journal of physiology. *Lung Cell Mol Physiol* (2011) 301:L99–L109. doi: 10.1152/ajplung.00398.2010

73. Lee REC, Walker SR, Savery K, Frank DA, Gaudet S. Fold-change of nuclear NF-κB determines TNF-induced transcription in single cells. *Mol Cell* (2014) 53:867–79. doi: 10.1016/j.molcel.2014.01.026

74. Lieber M, Smith B, Szakal A, Nelson-Rees W, Todaro G. A continuous tumor-cell line from a human lung carcinoma with properties of type II alveolar epithelial cells. *Int J Cancer* (1976) 17:62–70. doi: 10.1002/ijc.2910170110

75. Foster KA, Oster CG, Mayer MM, Avery ML, Audus KL. Characterization of the A549 cell line as a type II pulmonary epithelial cell model for drug metabolism. *Exp Cell Res* (1998) 243:359–66. doi: 10.1006/excr.1998.4172

76. Tari M, Manceau V, de Matha Salone J, Kobayashi A, Pastr´e D. Maucuer, a. U2AF65 assemblies drive sequence-specific splice site recognition. *EMBO Rep* (2019) 20:e47604. doi: 10.15252/embr.201847604

77. Gehring NH, Roignant J-Y. Anything but ordinary – emerging splicing mechanisms in eukaryotic gene regulation. *Trends Genet* (2021) 37:355–72. doi: 10.1016/j.tig.2020.10.008

78. Lin C-L, Taggart AJ, Lim KH, Cygan KJ, Ferraris L, Creton R, et al. RNA Structure replaces the need for U2AF2 in splicing. *Genome Res* (2016) 26:12–23. doi: 10.1101/gr.181008.114

79. Flemington EK, Flemington SA, O'Grady TM, Baddoo M, Nguyen T, Dong Y, et al. SpliceTools, a suite of downstream RNA splicing analysis tools to investigate mechanisms and impact of alternative splicing. *Nucleic Acids Res* (2023) 51:gkad111. doi: 10.1093/nar/gkad111

80. Schneider WM, Chevillotte MD, Rice CM. Interferon-stimulated genes: a complex web of host defenses. *Annu Rev Immunol* (2014) 32:513–45. doi: 10.1146/annurev-immunol-032713-120231

81. Ivashkiv LB, Donlin LT. Regulation of type I interferon responses. *Nat Rev Immunol* (2014) 14:36–49. doi: 10.1038/nri3581

82. Tian B, Zhao Y, Kalita M, Edeh CB, Paessler S, Casola A, et al. CDK9-dependent transcriptional elongation in the innate interferon-stimulated gene response to respiratory syncytial virus infection in airway epithelial cells. *J Virol* (2013) 87:7075–92. doi: 10.1128/JVI.03399-12

83. Smale ST. Selective transcription in response to an inflammatory stimulus. *Cell* (2010) 140:833–44. doi: 10.1016/j.cell.2010.01.037

84. Adelman K, Kennedy MA, Nechaev S, Gilchrist DA, Muse GW, Chinenov Y, et al. Immediate mediators of the inflammatory response are poised for gene activation through RNA polymerase II stalling. *Proc Natl Acad Sci United States America* (2009) 106:18207–12. doi: 10.1073/pnas.0910177106

85. Stender JD, Glass CK. Epigenomic control of the innate immune response. *Curr Opin Pharmacol* (2013) 13:582–7. doi: 10.1016/j.coph.2013.06.002

86. Jang MK, Mochizuki K, Zhou M, Jeong H-S, Brady JN, Ozato K. The bromodomain protein Brd4 is a positive regulatory component of p-TEFb and stimulates RNA polymerase II-dependent transcription. *Mol Cell* (2005) 19:523–34. doi: 10.1016/j.molcel.2005.06.027

87. Filippakopoulos P, Qi J, Picaud S, Shen Y, Smith WB, Fedorov O, et al. Selective inhibition of BET bromodomains. *Nature* (2010) 468:1067–73. doi: 10.1038/nature09504

88. Doroshow DB, Eder JP, LoRusso PM. BET inhibitors: a novel epigenetic approach. *Ann Oncol* (2017) 28:1776–87. doi: 10.1093/annonc/mdx157

89. Kim RS, Hasegawa D, Goossens N, Tsuchida T, Athwal V, Sun X, et al. The XBP1 arm of the unfolded protein response induces fibrogenic activity in hepatic stellate cells through autophagy. *Sci Rep* (2016) 6:39342. doi: 10.1038/srep39342

90. Chen G, Ribeiro CMP, Sun L, Okuda K, Kato T, Gilmore RC, et al. XBP1S regulates MUC5B in a promoter variant–dependent pathway in idiopathic pulmonary fibrosis airway epithelia. *Am J Respir Crit Care Med* (2019) 200:220–34. doi: 10.1164/rccm.201810-1972OC

91. Wang Q, Bu Q, Liu M, Zhang R, Gu J, Li L, et al. XBP1-mediated activation of the STING signalling pathway in macrophages contributes to liver fibrosis progression. *JHEP Rep* (2022) 4:100555. doi: 10.1016/j.jhepr.2022.100555

92. Micheli L, Leonardi L, Conti F, Buanne P, Canu N, Caruso M, et al. PC4 coactivates MyoD by relieving the histone deacetylase 4-mediated inhibition of myocyte enhancer factor 2C. *Mol Cell Biol* (2005) 25:2242–59. doi: 10.1128/MCB.25.6.2242-2259.2005

93. Chang M, Zhang Y, Hui Z, Wang D, Guo H. IFRD1 regulates the asthmatic responses of airway ***via*** NF-κB pathway. *Mol Immunol* (2020) 127:186–92. doi: 10.1016/j.molimm.2020.09.010

94. Gu Y, Harley ITW, Henderson LB, Aronow BJ, Vietor I, Huber LA, et al. IFRD1 polymorphisms in cystic fibrosis with potential link to altered neutrophil function. *Nature* (2009) 458:1039–42. doi: 10.1038/nature07811

95. Chen J, Chen L-F. Methods to detect NF-κB acetylation and methylation. *Methods Mol Biol Clifton N.J* (2015) 1280:395–409. doi: 10.1007/978-1-4939-2422-6_24

96. David CJ, Boyne AR, Millhouse SR, Manley JL. The RNA polymerase II c-terminal domain promotes splicing activation through recruitment of a U2AF65–Prp19 complex. *Genes Dev* (2011) 25:972–83. doi: 10.1101/gad.2038011

97. Gegonne A, Chen Q-R, Dey A, Etzensperger R, Tai X, Singer A, et al. Immature CD8 single-positive thymoc a molecularly distinct subpopulation, selectively dependent on BRD4 for their differentiation. *Cell Rep* (2018) 24:117–29. doi: 10.1016/j.celrep.2018.06.007

98. Kukurba KR, Montgomery SB. RNA Sequencing and analysis. *Cold Spring Harbor Protoc* (2015) 2015:951–69. doi: 10.1101/pdb.top084970

99. Stark R, Grzelak M, Hadfield J. RNA Sequencing: the teenage years. *Nat Rev Genet* (2019) 20:631–56. doi: 10.1038/s41576-019-0150-2

100. Ghazalpour A, Bennett B, Petyuk VA, Orozco L, Hagopian R, Mungrue IN, et al. Comparative analysis of proteome and transcriptome variation in mouse. *PloS Genet* (2011) 7:e1001393. doi: 10.1371/journal.pgen.1001393

101. Haider S, Pal R. Integrated analysis of transcriptomic and proteomic data. *Curr Genomics* (2013) 14:91–110. doi: 10.2174/1389202911314020003

102. Brunner A-D, Thielert M, Vasilopoulou C, Ammar C, Coscia F, Mund A, et al. Ultra-high sensitivity mass spectrometry quantifies single-cell proteome changes upon perturbation. *bioRxiv* (2021) 2020:12.22.423933. doi: 10.1101/2020.12.22.423933

103. Mann M, Brasier AR. Evolution of proteomics technologies for understanding respiratory syncytial virus pathogenesis. *Expert Rev Proteomics* (2021) 18:379–94. doi: 10.1080/14789450.2021.1931130

104. Smith LM, Kelleher NL. Proteoform: a single term describing protein complexity. *Nat Methods* (2013) 10:186–7. doi: 10.1038/nmeth.2369

105. Bayega A, Wang YC, Oikonomopoulos S, Djambazian H, Fahiminiya S, Ragoussis J. Transcript profiling using long-read sequencing technologies. *Methods Mol Biol* (2018) 1783:121–47. doi: 10.1007/978-1-4939-7834-2_6

106. Amarasinghe SL, Su S, Dong X, Zappia L, Ritchie ME, Gouil Q. Opportunities and challenges in long-read sequencing data analysis. *Genome Biol* (2020) 21:30. doi: 10.1186/s13059-020-1935-5

107. Doerr A. Top-down mass spectrometry. *Nat Methods* (2008) 5:24–4. doi: 10.1038/nmeth1162

108. Cai W, Tucholski TM, Gregorich ZR, Ge Y. Top-down proteomics: technology advancements and applications to heart diseases. *Expert Rev Proteomics* (2016) 13:717–30. doi: 10.1080/14789450.2016.1209414

109. Melby JA, Roberts DS, Larson EJ, Brown KA, Bayne EF, Jin S, et al. Novel strategies to address the challenges in top-down proteomics. *J Am Soc Mass Spectrometry* (2021) 32:1278–94. doi: 10.1021/jasms.1c00099